The Astrophysical Journal, 663:505–515, 2007 July 1

SWIFT X-RAY OBSERVATIONS OF CLASSICAL NOVAE

J.-U. Ness,[1] G. J. Schwarz,[2] A. Retter,[3] S. Starrfield,[1] J. H. M. M. Schmitt,[4] N. Gehrels,[5]
D. Burrows,[6] and J. P. Osborne[7]

Received 2006 October 17; accepted 2007 March 9

ABSTRACT

The new γ-ray burst (GRB) mission *Swift* has obtained pointed observations of several classical novae in outburst. We analyzed all the observations of classical novae from the *Swift* archive up to 2006 June 30. We analyzed usable observations of 12 classical novae and found 4 nondetections, 3 weak sources, and 5 strong sources. This includes detections of two novae exhibiting spectra resembling those of supersoft X-ray binary source spectra (SSS), implying ongoing nuclear burning on the white dwarf surface. With these new *Swift* data, we add to the growing statistics of the X-ray duration and characteristics of classical novae.

Subject headings: novae, cataclysmic variables — stars: individual (V574 Pup, V382 Nor, V1663 Aql, V5116 Sgr, V1047 Cen, V476 Sct, V477 Sct, Nova LMC 2005, V1494 Aql, V4743 Sgr, V1188 Sco) — X-rays: stars

Online material: color figure

1. INTRODUCTION

The explosions of classical novae (CNe) occur in close binary star systems where mass is accreted onto a white dwarf (WD) from a low-mass secondary star. The accreted material gradually becomes degenerate, and when temperatures become high enough and the pressure at the bottom of the accreted envelope exceeds a certain value, a thermonuclear runaway results. Enough energy is deposited in the accreted material to eject some fraction from the WD. The outburst can last several months to years, and CNe become active in X-rays at some time during their outburst (e.g., Pietsch et al. 2005, 2006). The relatively slow evolution makes CNe ideal targets for *Swift*, as no accurate times of observation need to be scheduled, and they can thus be observed with great flexibility.

The evolution of X-ray emission starts soon after outburst when the expanding nova envelope is still small and dense. The energy peak during this earliest time, called the "fireball" phase (Shore et al. 1994; Schwarz et al. 2001), is expected to occur at X-ray wavelengths. This phase is extremely difficult to observe, since it is predicted to last only a few hours after the beginning of the outburst, so it is over before the nova can be discovered in the optical. As the envelope increases in size and cools, the opacity increases, shifting the radiation toward wavelengths longer than the hydrogen absorption edge at 13.6 eV (911 Å). The expanding, cooling envelope gives rise to the large and rapid increase in the visual luminosity of the nova. Around the time of visual maximum, X-rays from the underlying WD are trapped inside the large column density of the ejecta. However, shocks may develop within the early expanding ejecta, producing a hard, sub-Eddington luminosity, X-ray spectral energy distribution (e.g., V382 Vel; Orio et al. 2001b; Mukai & Ishida 2001). As the shell continues to expand, the density and opacity drop, and X-rays emitted from the surface of the WD eventually become visible (Krautter et al. 1996). Soft X-ray emission originates from hot layers produced by the nuclear burning of the remaining accreted material on the WD. This material burns in equilibrium at a high but constant luminosity $\propto L_{\rm Eddington}$ (Gallagher & Starrfield 1978). The spectral energy distribution resembles that of supersoft X-ray sources (SSS; e.g., Cal 83; Paerels et al. 2001; Lanz et al. 2005).

Recent observations of novae during this phase show that the flux can also be highly variable on short timescales (see, e.g., Ness et al. 2003; J. P. Osborne et al. 2007, in preparation). The duration of this SSS phase is predicted to be inversely proportional to the WD mass (Starrfield 1991), but a review of the *ROSAT* X-ray sky survey (Orio et al. 2001a) showed that the timescale is much shorter than predicted, implying either that the masses of WDs in CNe are much higher than commonly assumed or that the X-ray turnoff is a function of more than the WD mass. A different approach was proposed by Greiner et al. (2003), who found from the available data that systems with shorter orbital periods display long durations of supersoft X-ray phases, while long-period systems show a very short or no SSS phase at all. They speculate that shorter periods may be related to a higher mass transfer rate (e.g., by increased irradiation) and thus to the amount of material accreted before the explosion.

Another source of X-ray emission from novae is emission lines from material that has been radiatively ionized. These lines are expected to be present during the entire evolution, but are usually only observed once the nuclear fuel is consumed and the bright continuous SSS spectrum (that outshines the emission lines) fades. The ejecta quickly recombine until a collisional equilibrium is reached. This equilibrium reflects the kinetic temperature distribution of the plasma, and the elemental abundances can be derived (Ness et al. 2005). This phase is called the nebular phase and is also seen at other wavelengths (Shore et al. 2003). In some cases, X-ray emission from lines has been observed earlier, either prior to the SSS phase, superimposed on the SSS spectrum (e.g., V1494

[1] School of Earth and Space Exploration, Arizona State University, Tempe, AZ 85287-1404: Jan-Uwe.Ness@asu.edu, sumner.starrfield@asu.edu.
[2] Department of Geology and Astronomy, West Chester University, 750 S. Church Street, West Chester, PA 19383.
[3] Department of Astronomy and Astrophysics, Penn State University, 525 Davey Lab, University Park, PA 16802-6305.
[4] Hamburger Sternwarte, Gojenbergsweg 112, 21029 Hamburg, Germany.
[5] NASA/Goddard Space Flight Center, Greenbelt, MD 20771.
[6] Department of Astronomy and Astrophysics, Penn State University, University Park, PA 16802.
[7] Department of Physics and Astronomy, University of Leicester, Leicester, LE1 7RH, UK.

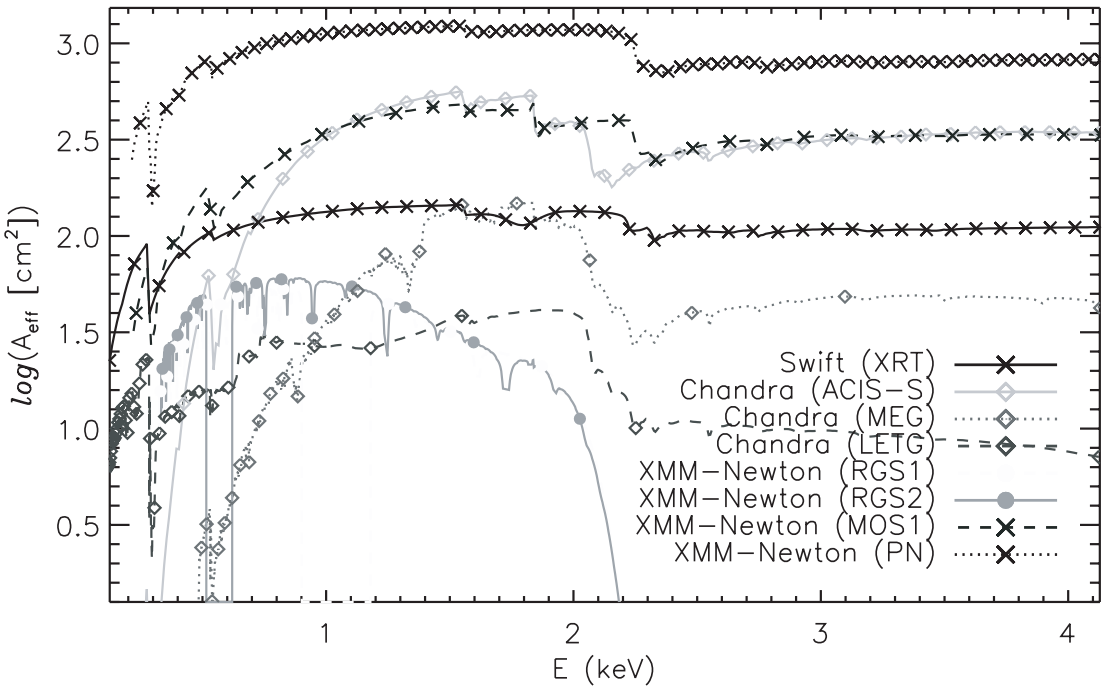

FIG. 1.—Comparison of XRT effective areas of *Swift* with other X-ray instruments that are sensitive in the same spectral region. None of the *Chandra* or *XMM-Newton* gratings have a higher effective area than the XRT. The CCD detectors, ACIS-S (*Chandra*) and EPIC (PN/MOS1; *XMM-Newton*), have higher effective areas. The spectral resolution of the XRT is similar to either the ACIS or EPIC detectors, but the spectral resolution of the gratings is far superior. [*See the electronic edition of the Journal for a color version of this figure*.]

Aql), or during times of extreme variability, when the SSS emission suddenly declines before recovery (e.g., V4743 Sgr; Ness et al. 2003).

X-ray observations provide important clues to the properties and dynamics of novae. The evolution of the SSS depends on the WD mass, the mass loss rate (via radiatively driven winds or common envelope mass loss), the amount of ejected material, the amount of material remaining on the WD, the binary separation, and the expansion velocity of the ejecta. Analysis of the X-ray emission can also provide insight into the composition of the ejecta. Unfortunately, only a few novae have been studied extensively in X-rays, with much of the recent information coming from *Chandra* and *XMM-Newton*. Now, with *Swift*, we have the possibility of studying novae in large numbers in order to assess statistical properties. *Swift* also allows for coordination of higher resolution observations with *Chandra* and *XMM-Newton*, since it has always been difficult to predict the brightness in X-rays and to estimate the optimal exposure time for X-ray observations with the gratings.

In this paper, we discuss the *Swift* XRT instrument briefly in § 2.1. Since interstellar absorption plays an important role in Galactic novae, we discuss the expected effects on the detection of SSS in § 2.2. In § 3 we sort the observations by nondetections and detections of weak and strong sources based on our extraction statistics, detailed in the Appendix. We discuss our results in § 4 and expand on the type of X-ray emission that was detected in the *Swift* observations.

2. *SWIFT* OBSERVATIONS

2.1. *The Instrument*

Our entire data set has been obtained with the X-ray Telescope (XRT) aboard *Swift* (Burrows et al. 2005). The XRT instrument is a CCD detector behind a Wolter Type I grazing incidence mirror consisting of 12 nested shells. The field of view covers $23.6' \times 23.6'$, imaged on a detector with 600×600 pixels, and thus each pixel corresponds to $2.36''$. The point spread function (PSF) can be parameterized, and source radii of 10 pixels and 5 pixels include 80.5% and 60.5% of the total energy, respectively (Moretti et al. 2004). The positional accuracy is $2.5''$, or one pixel. The energy range covers 0.2–10 keV with the full width at half maximum (FWHM) energy resolution varying from ~50 eV at 0.1 keV to ~190 eV at 10 keV. In Figure 1, we show a comparison of effective areas of *Swift*, *Chandra*, and *XMM-Newton*. In general, the *Swift* XRT has a smaller effective area than the *Chandra*/ACIS-S except at low energies (long wavelengths), where the *Chandra*/ACIS-S suffers from large calibration uncertainties. The EPIC detectors PN and MOS1 (*XMM-Newton*) have 50% and 20% higher effective areas, respectively. The XRT, ACIS, and EPIC instruments have similar spectral resolution. The XRT effective area is larger than that of the gratings aboard *Chandra* (LETG and MEG) and *XMM-Newton* (RGS1 and RGS2), but the XRT spectral resolution is much lower. Figure 1 demonstrates that the XRT is an ideal instrument for exploring the emission level of novae using reasonable exposure times (~3–6 ks). Once a nova is detected with *Swift* and found to be sufficiently bright, additional observations can be requested with the high-resolution grating instruments aboard *Chandra* and *XMM-Newton* to obtain detailed spectral information. The detector was operated in photon counting (PC) mode, which provides two-dimensional imaging, spectral information, and 2.5 s time resolution.

2.2. *Observability of the Supersoft Source Phase in Classical Novae*

Unfortunately, many Galactic CNe have large extinction rates, which has a pronounced effect on the observability of the SSS emission. To illustrate this, we attenuate a series of Cloudy models (Ferland et al. 1998) through different amounts of H I column

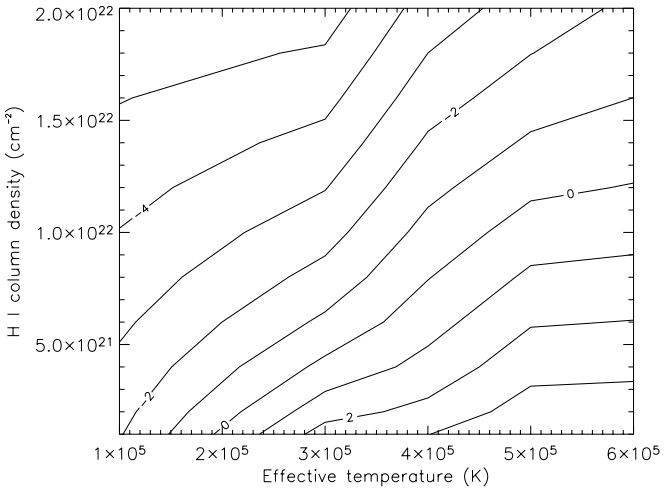

FIG. 2.—Contour plot of the log *Swift* counts predicted with a 1 ks observation from a SSS as a function of temperature (Cloudy model) and interstellar extinction ($N_{\rm H}$) for a source at a distance of 1 kpc.

densities and determine the resulting *Swift* counts. The models use non-LTE atmospheres by Rauch (1997) for planetary nebula nuclei with effective temperatures in the range of $(1-6)\times10^5$ K (8–50 eV) as the input source. The model luminosity was fixed at 10^{38} erg s^{-1}, which is approximately the Eddington luminosity for a 1 $M_\odot$ star. The spectral energy distributions were attenuated by H I column densities in the range $(1-20)\times10^{21}$ cm^{-2} and then converted to *Swift* net count rates using the effective area of the XRT and scaled to a 1 ks exposure at 1 kpc. The logarithms of the expected total XRT counts are shown as contours in Figure 2. As expected, the ability to detect a SSS is highly dependent on $N_{\rm H}$ and the source's effective temperature. Sources with low temperatures are more difficult to detect if significant $N_{\rm H}$ absorption takes place. Without long (>10 ks) exposures, $N_{\rm H}\sim10^{22}$ cm^{-2} is the highest number that allows a detection of SSS emission at a 1 kpc distance with *Swift*. Since most novae are further away than 1 kpc, the situation is even worse.

2.3. *Targets*

Although primarily a mission to study the temporal evolution of γ-ray bursts (GRBs), *Swift* also provides targets of opportunity (ToO) observations for non-GRB events. Through ToO observations, we have obtained X-ray observations of nine recent (<1–2 years since outburst) and three older (>3 years) CNe. We consider all observations, although those of V1188 Sco on 2006 May 21 (o/00035191001) and of V574 Pup taken on 2005 July 26 (o/00035170004) were extremely short with hardly any signal. Table 1 provides a list of important physical parameters associated with these novae, including the maximum visual magnitudes, the date of discovery, the time to decline 2 mag from maximum (t_2), the early measured expansion velocities, $E(B-V)$ reddening values, H I column densities, and distances.

3. ANALYSIS OF THE *SWIFT* XRT DATA

Currently the *Swift* archive contains 27 observations of 12 novae obtained with the XRT instrument (see § 2.1). We analyzed the data using the *Swift* reduction packages in HEAsoft version 6.06[8] and the latest calibration data (ver. 20060427). We started with the photon event files (level 2) that are available in the public *Swift* archive and carried out three statistical tests to determine if the sources were detected. We then calculated count rates or upper limits in cases where no detections can be claimed. The first criterion is the formal detection likelihood from comparison of the number of counts measured in the source extraction region (circular with a 10 pixel radius around the expected sky position) with the background extraction region (annulus around source extraction region with an inner of radius 10 pixels and an outer radius of

[8] See http://swift.gsfc.nasa.gov/docs/software/lheasoft/.

TABLE 1
BASIC NOVA PARAMETERS

Object	$V_{\rm max}$ (mag)	Date[a]	t_2[b] (days)	$v_{\rm exp}$[c] (km s^{-1})	$E(B-V)$ (mag)	$N_{\rm H}$[d] (cm^{-2})	Distance (kpc)	References[e]
V574 Pup	8	2004 Nov 11	13	650H, 860P	0.5	6.5E21	3.20	1, 2, 3
V382 Nor	9	2005 Mar 19	13	1100P	0.6–1.1	1.8E22	13.80	3, 3, 3
V1663 Aql	10.5	2005 Jun 10	16	700P	~2	1.8E22	5.5 ± 1	4, 5, 4
V5116 Sgr	<8	2005 Jul 04	20	1300P	0.24 ± 0.08	1.6E21	11.30	3, 3, 3
V1188 Sco	8.9	2005 Jul 26	12	1730H, 4000Z	~1?	5.0E21	7.5	3, 3, 3
V1047 Cen	8.83	2005 Sep 04	?	850H	3.3?	1.6E22	?	–, 3, –
V476 Sct	10.9	2005 Sep 30	15	1200H	1.9 ± 0.1	1.1E22	4 ± 1	6, 6, 6
V477 Sct	10.4	2005 Nov 10	3	2700H, 6000Z	>1.3	4.8E21	11	7, 7, 7
Nova LMC 2005	12.6	2005 Nov 27	?	...	0.15	6.3E20	50	3, 3, 3
V723 Cas	7.1	1995 Dec 17	slow	700H	~0.5	2.4E21	4	–, 8, 9
V1494 Aql	4	1999 Dec 03	6.6 ± 0.5	1300H, 1850P	0.6 ± 0.1	4.2E21	1.6 ± 0.2	10, –, 11
V4743 Sgr	5	2002 Sep 20	9	2400H	low?	1.4E21	6.3	3, –, 12

[a] Date of visual maximum.
[b] Time to decline 2 mag from maximum.
[c] Expansion velocity. Taken from early IAU circulars. Trailing letters indicate how the velocity was measured: H = full width at half-maximum, P = P Cygni absorption, Z = full width at zero intensity.
[d] The H I column densities were obtained from the Heasarc NH tool. They are the line-of-sight column densities through the entire Galaxy toward the coordinates of each object.
[e] References for t_2, $E(B-V)$, and distance.

REFERENCES.—(1) Siviero et al. 2005; (2) R. J. Rudy 2006, private communication; (3) t_2 from AAVSO light curve and IAU circulars, $E(B-V)$ using van den Bergh & Younger (1987) and the $(B-V)$ color evolution or assuming $E(B-V)\sim N_{\rm H}/4.8\times10^{21}$ cm^{-2}, and distance using the M_V vs. t_2 relationship of Della Valle & Livio (1995); (4) Lane et al. 2006; (5) Puetter et al. 2005; (6) Munari et al. 2006a, Perry et al. 2005; (7) Munari et al. 2006b; (8) Munari et al. 1996; (9) Iijima et al. 1998; (10) Kiss & Thomson 2000; (11) Iijima & Esenoglu 2003; (12) Lyke et al. 2002.

TABLE 2

MEASURED COUNT RATES IN OUR SAMPLE

Observation Start Date	Δt[a] (days)	Exposure (ks)	Source (counts)[b]	Background (counts)[b]	Count Rate[b,c] (counts ks^{-1})	$R_{1/2}$[d] (%)
V574 Pup						
2005 May 20 (o/00035170001).....	175	1.0	10	0.4	12.0 ± 4.0	60
2005 May 25 (o/00035170003).....	180	1.9	22	0.4	14.0 ± 3.0	77
2005 May 26 (o/00035170004).....	...	0.01	0	0	0	0
2005 Jul 29 (o/00035170005).....	245	1.1	15	0.3	16.0 ± 4.0	67
2005 Jul 30 (o/00035170006).....	246	7.1	51	2.1	8.5 ± 1.3	73
2005 Aug 6 (o/00035170007).....	253	7.8	57	2.0	8.7 ± 1.2	67
2005 Aug 9 (o/00035170008).....	256	2.2	22	0.6	12.0 ± 3.0	64
2005 Aug 10 (o/00035170009).....	257	2.8	18	0.8	7.8 ± 2.0	67
2005 Aug 11 (o/00035170010).....	258	1.8	11	0.5	7.3 ± 2.5	56
2005 Aug 17 (o/00035170011).....	264	4.7	34	1.2	8.6 ± 1.6	79
V382 Nor						
2006 Jan 26 (o/00035195002).....	313	6.1	72	4.0	14.0 ± 2.0	75
V1663 Aql						
2005 Aug 15 (o/00035193001).....	66	1.3	9	0.3	8.6 ± 3.3	78
2006 Mar 4 (o/00035193002).....	267	6.5	3	1.1	<0.5[c]	0
V5116 Sgr						
2005 Aug 29 (o/00035192001).....	56	3.1	5	2.0	1.2 ± 1.0	80
V1188 Sco						
2006 Apr 21 (o/00035191001).....	98	0.2	1	0.1	<7[c]	0
2006 Jun 17 (o/00035191002).....	124	5.0	3	2.3	<9.1[c]	33
V1047 Cen						
2005 Sep 11 (o/00035231001).....	66	3.9	19	1.3	5.6 ± 1.5	53
2006 Jan 23 (o/00035231002).....	141	5.3	53	3.1	11.0 ± 2.0	72
V476 Sct						
2006 Feb 12 (o/00035229001).....	135	3.8	2	1.0	<8.2[c]	50
V477 Sct						
2006 Mar 7 (o/00035230001).....	117	6.2	15	1.8	2.7 ± 0.8	87
2006 Mar 15 (o/00035230002).....	125	4.7	8	1.3	1.8 ± 0.8	50
Nova LMC 2005						
2005 Dec 2 (o/00030348001).....	5	0.1	0	0.1	<1.0[c]	0
2005 Dec 1 (o/00030348002).....	4	4.1	1	1.3	<8.6[c]	100
2005 Dec 2 (o/00030348003).....	5	3.9	2	1.2	<8.7[c]	100
2005 Dec 3 (o/00030348004).....	6	5.7	1	1.7	<7.0[c]	50
V723 Cas						
2006 Jan 31 (o/00030361001).....	3698	6.9	147	1.7	26.0 ± 2.0	69
V1494 Aql						
2006 Mar 10 (o/00035222001).....	2289	1.4	0	0.3	<1.4[c]	0
2006 Mar 13 (o/00035222002).....	2292	1.2	0	0.2	<1.4[c]	0
2006 May 19 (o/00035222003).....	2359	2.5	1	0.5	<1.0[c]	100
V4743 Sgr						
2006 Mar 8 (o/00035221001).....	1265	5.8	267	2.3	27.0 ± 2.0	70

[a] Interval between visual maximum and the XRT observation in days.
[b] Per detect cell (10 pixel radius); count rates with 1 σ uncertainties.
[c] 95.5% upper limit.
[d] Fraction of counts within 5 pixels (%).

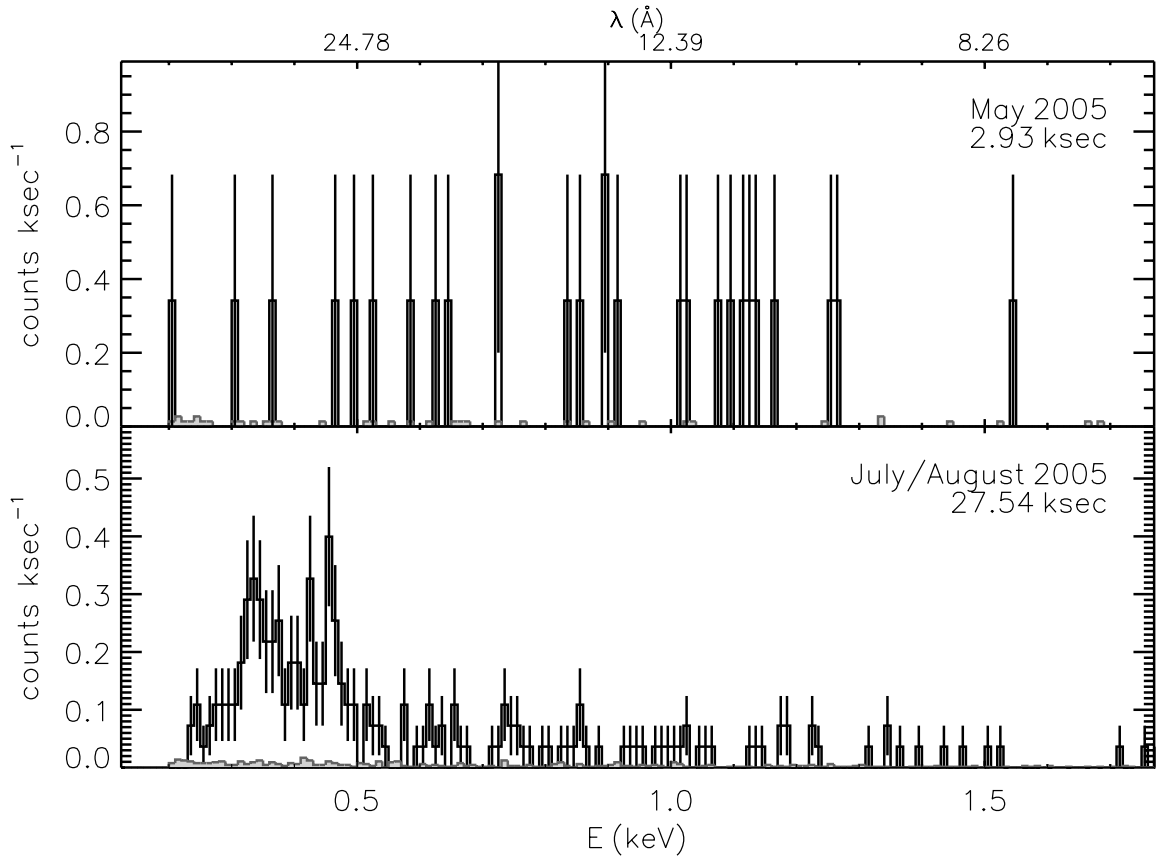

FIG. 3.—Grouped XRT observations of V574 Pup comparing the May 2005 (*top panel*) and the July through August data sets (*bottom panel*). The comparison shows that V574 Pup has evolved from a hard early spectrum (*top panel*) into a SSS spectrum (*bottom panel*). The count rate is higher in the top panel, which may be due either to the higher sensitivity of the detector at higher energies or the higher amounts of absorption at soft energies.

100 pixels). We next determined whether there was a concentration of counts near the center of the source extraction region. Finally, we compared the spectral distributions of photons in the source and background extraction regions, but this is only a soft criterion, as similar spectral distributions do not rule out the presence of a source. We present our statistical methods in more detail in the Appendix to justify our tests.

In Table 2, we provide all the *Swift* observational data, including observation date, time since visual maximum, exposure time, number of counts in the source and background extraction regions, and either the net source count rate per detect cell with 1 σ uncertainty or the upper limit.

3.1. *Nondetections, Failure of All Criteria*

Only upper limits could be established for the observations of V476 Sct, V1188 Sco, Nova LMC 2005, and V1494 Aql. We found only a marginal detection in the *Chandra* observation of V1494 Aql five years prior to the *Swift* observations (see § 3.4). We used the proposal planning tool PIMMS in order to convert the *Chandra* count rate into an expected *Swift* XRT count rate. With various model assumptions, PIMMS predicts more than 0.04 XRT counts s^{-1}, while we measured less than 0.0014 counts s^{-1} in each observation (Table 2). This implies that the source has faded by at least a factor of 30 within five years.

3.2. *Weak Sources* <0.01 *Counts per Second*

V1663 Aql was the first nova observed by *Swift*. Unfortunately, the first planned observation was truncated by a GRB after only 1.25 ks. Nevertheless, we find a clear detection and a strong concentration of counts toward the center (Table 2). The source spectrum is similar to the background spectrum, but that does not rule out a detection. The spectrum is extremely weak and no conclusion can be drawn. A second observation seven months later was longer, but yielded only an upper limit, which implies a fading of the source. Neither of our other two criteria supported a detection.

For V5116 Sgr, we only found a marginal (formal 93%) detection with a concentration of photons toward the center. The spectrum is too weak to apply our source-background comparison criterion.

Two observations of V477 Sct were carried out eight days apart and resulted in two detections with a likelihood >99%. The first observation suggests a weak source with a clear concentration toward the center and a much softer spectrum than that of the instrumental background. The second observation reveals a lower count rate, lower detection likelihood, and a less clear concentration of photons toward the center. While this implies variability or that the source has faded over the eight-day interval, within the 1 σ errors, the count rate is consistent with that of the first observation. Neither spectrum allows quantitative analysis.

3.3. *Strong Sources* >0.01 *Counts per Second*

V574 Pup, V382 Nor, V1047 Cen, V723 Cas, and V4743 Sgr were detected by *Swift*. The spectrum of V382 Nor is hard, whereas the background is softer. There appears to be some excess emission at wavelengths of prominent emission lines (e.g., 0.92 keV, Ne IX; 1.02 keV, Ne X; and 0.83 keV, Fe XVII), but a firm identification of

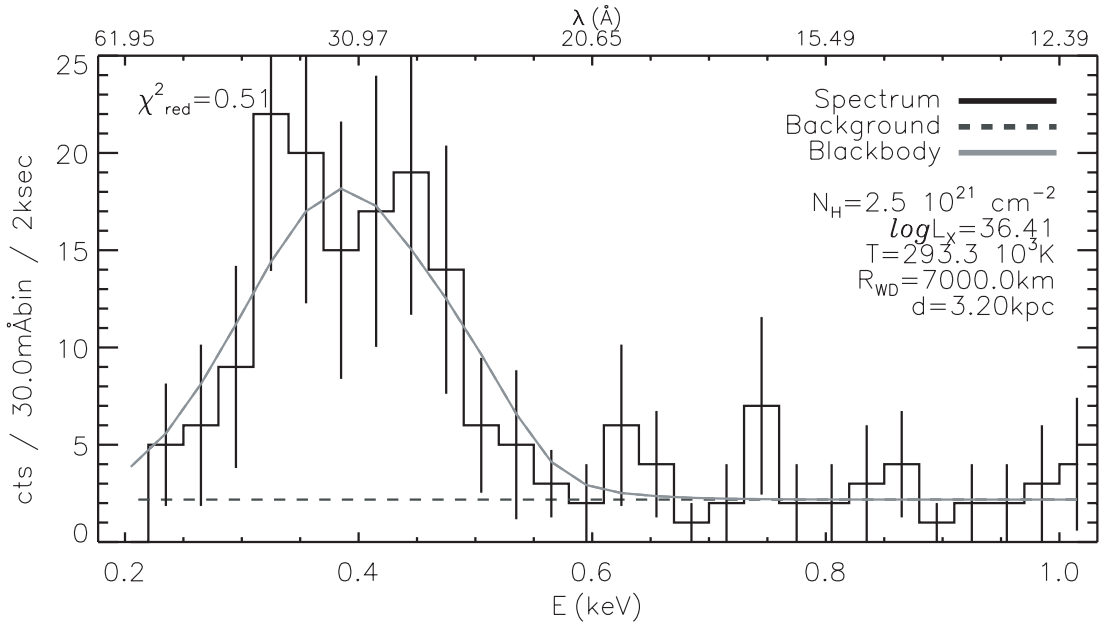

FIG. 4.—Grouped and rebinned XRT spectrum of V574 Pup covering July 2005 to August 2005 (shown in the bottom panel of Fig. 3). The histogram (plus error bars) gives the observed spectrum, and a smooth line showing the best-fit blackbody model is overplotted (parameters given in legend).

these lines is not possible with the existing data. There is also emission at energies with no well-known emission lines, particularly at high energies. The observed spectrum is too faint to derive any quantitative conclusions.

We obtained very clear detections of V1047 Cen. In the first observation of November 2005, the photons are clearly concentrated toward the center, and the energy distribution is very different from the soft background. Two months later, the detection is even stronger, and the spatial as well as spectral distributions clearly support a detection. The count rate doubled from 5.6 counts ks^{-1} on 2005 November 9 to 11 counts ks^{-1} on 2006 January 23. The spectrum appears hard, but there are too few counts to derive any spectral properties.

The remaining novae were sufficiently bright to obtain spectral confirmation that they were detected during the SSS phase. More detailed analyses of these spectra, including additional *Swift* observations and supporting optical and near-IR spectra, is left for future papers. Here we only provide a brief analysis of the current *Swift* data sets.

V574 Pup was first observed in late May 2005. It was then observed multiple times from the end of July to mid-August 2005, as it was perfectly positioned to cool the XRT detectors between GRB observations. In all nine observations, it was clearly detected with a high degree of significance (see Table 2). V574 Pup had an average of 7–14 counts ks^{-1} in each observation. The individual observations were too short for analysis, so we combined them, yielding a higher signal-to-noise ratio. We grouped the spectra by summing the number of counts and the number of background counts in each spectral bin. We calculated exposure time–weighted effective areas from the individual extracted effective areas.

However, during the 50 days between the May 26 and July 29 observations, significant evolution probably occurred, which we would miss by combining all spectra together. In order to search for any evolution, we grouped the first two observations from May 2005 and the remaining observations from July and August 2005. These are shown in Figure 3. The summed spectra of the two early observations shows a uniform distribution with energy and may be an underexposed emission-line spectrum. Unfortunately, we do not have any more data from this time period to increase the signal-to-noise ratio. The later observations sum up to what appears to be a continuous spectrum in the range 0.3–0.5 keV (25–45 Å). This spectrum resembles that of a SSS. We carried out a blackbody fit using the most recent XRT response matrices (ver. 8) and assuming an emitting radius of 7000 km. We found a satisfactory fit (Fig. 4) with the parameters $T_{\rm eff} = (293 \pm 10) \times 10^3$ K (25.2 ± 1 eV) and $N_{\rm H} = (2.5 \pm 0.6) \times 10^{21}$ cm^{-2} (1 σ uncertainty ranges). We fixed the radius because no unique solution could be found with a variable radius. The uncertainties include variations of the radius between 7000 and 9000 km.

The XRT spectrum of V4743 Sgr is faint, and no spectral features can be identified. We also found no features in the RGS observation taken in September 2004 (see below). While the XRT count rates of V4743 Sgr and V723 Cas are similar, the spectra are different (Fig. 5). V723 Cas shows a clear peak occurring at 0.4 keV (31 Å). Ness et al. (2006) reported that the spectrum resembled a SSS, and they were able to fit a blackbody model. We repeated these fits using the updated XRT response matrices (ver. 8) and show the best-fit model in Figure 6. We fixed the radius at 7000 km, but included variations up to 9000 km in the calculation of the 1 σ uncertainty ranges. We find $T_{\rm eff} = (371 \pm 15) \times 10^3$ K (32 ± 2 eV) and $N_{\rm H} = (3.3 \pm 0.4) \times 10^{21}$ cm^{-2}. V723 Cas is now, after 11 years, the oldest Galactic nova that is still active. Such a long duration of the SSS phase is unusual for a classical nova, and there is a possibility that the nova has transitioned into a SSS, such as Cal 83. Our observations of this interesting source are continuing.

3.4. *Supplemental Observations*

In addition to the *Swift* observations, we extracted unpublished X-ray observations from the *Chandra* and *XMM-Newton* archives. A series of *Chandra* observations of V1494 Aql was carried out, and we extracted the last observation (LETGS, ObsID 2681 [obs/2681]), taken 727 days after outburst (2001 November 28). The source was only detected in the zeroth order on the HRC-S detector, but no dispersed spectrum could be extracted. We found

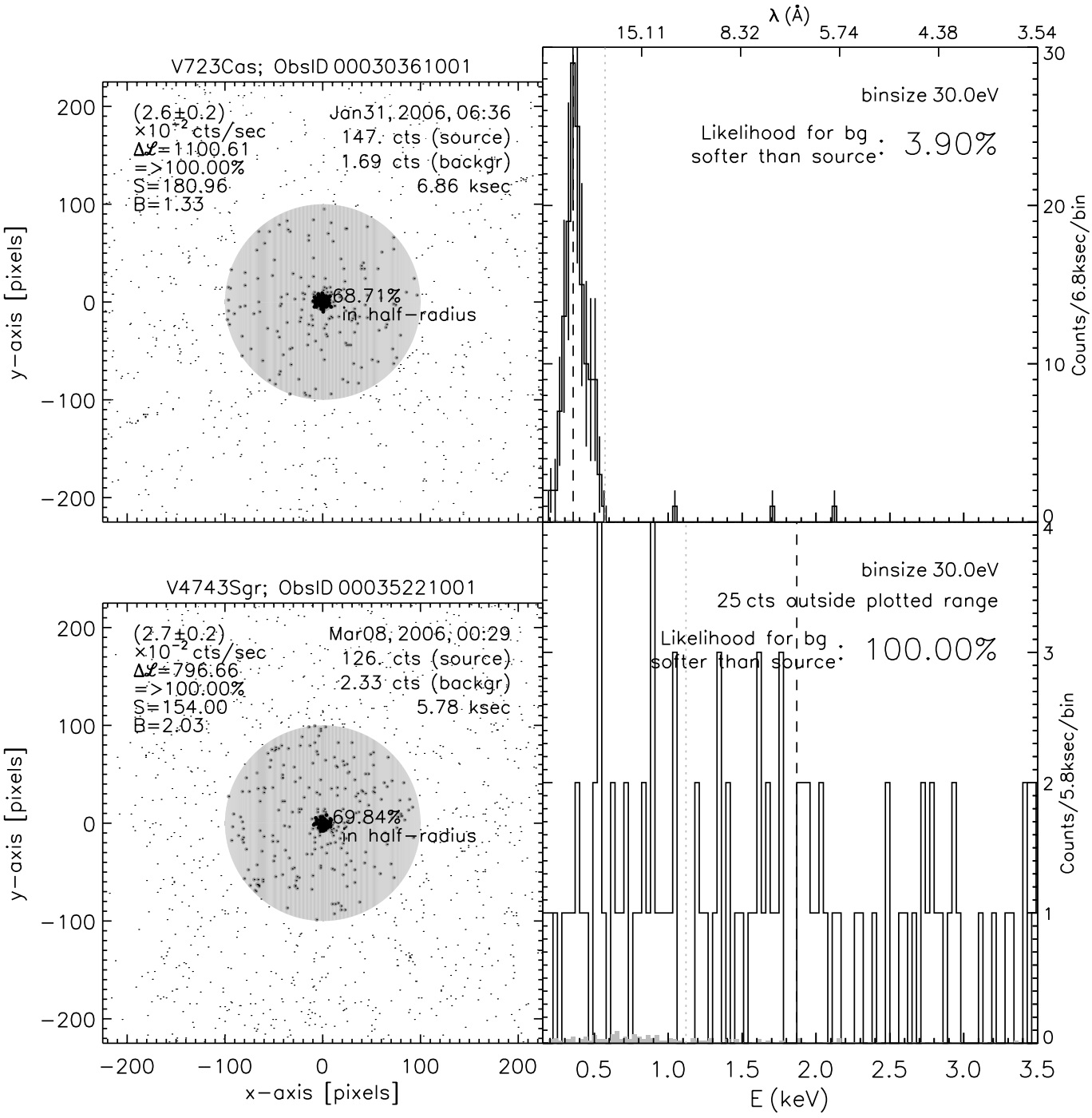

FIG. 5.—Illustration of extraction of counts for V723 Cas (*top*) and V4743 Sgr (*bottom*). *Left panels*: We show the recorded photon positions and mark the source extraction region with dark shading and the background extraction region (annulus with inner radius 10 pixels and outer radius 100 pixels) with light shading. The count rate, detection likelihood, and the model parameters S and B determined from eq. (A1) are given in the upper left. Observation date, number of source- and background-counts per detect cell, and exposure time are given in the upper right. The percentage of source counts that reside within a 25% area (radius of 5 pixels) is given to the right of the source extraction region to demonstrate the concentration of counts toward the center of the source extraction region. *Right panels*: Spectral information of the source (*black lines*) and background (scaled to the area of the source extraction region; light shadings). The likelihood of the background spectrum being softer than the source spectrum is estimated by drawing 1000 random sample spectra, with the same number of source counts (147, *top panel*; 126, *bottom panel*), out of the background ($1.69 \times 99 = 167.31$ counts, *top panel*; $2.33 \times 99 = 230.67$ counts, *bottom panel*) and counting the number of cases where the median energy for each sample spectrum is lower than that of the source spectrum. Values much different than 50% are a soft criterion for a source detection.

56 counts on a background of 10, corresponding to an HRC count rate of 0.02 ± 0.003 counts s^{-1} and a 14 σ detection. Unfortunately, the HRC detector does not provide the energy resolution to construct a spectrum, and no spectrum can be constructed from the dispersed photons, as the background is too high.

We further analyzed *XMM-Newton* observations of Nova LMC 2005 taken 243 days after outburst (ObsID 0311591201, 2006 July 18) and of V4743 Sgr 1470 days after outburst (ObsID 0204690101, 2004 September 30). Nova LMC 2005 was again not detected.

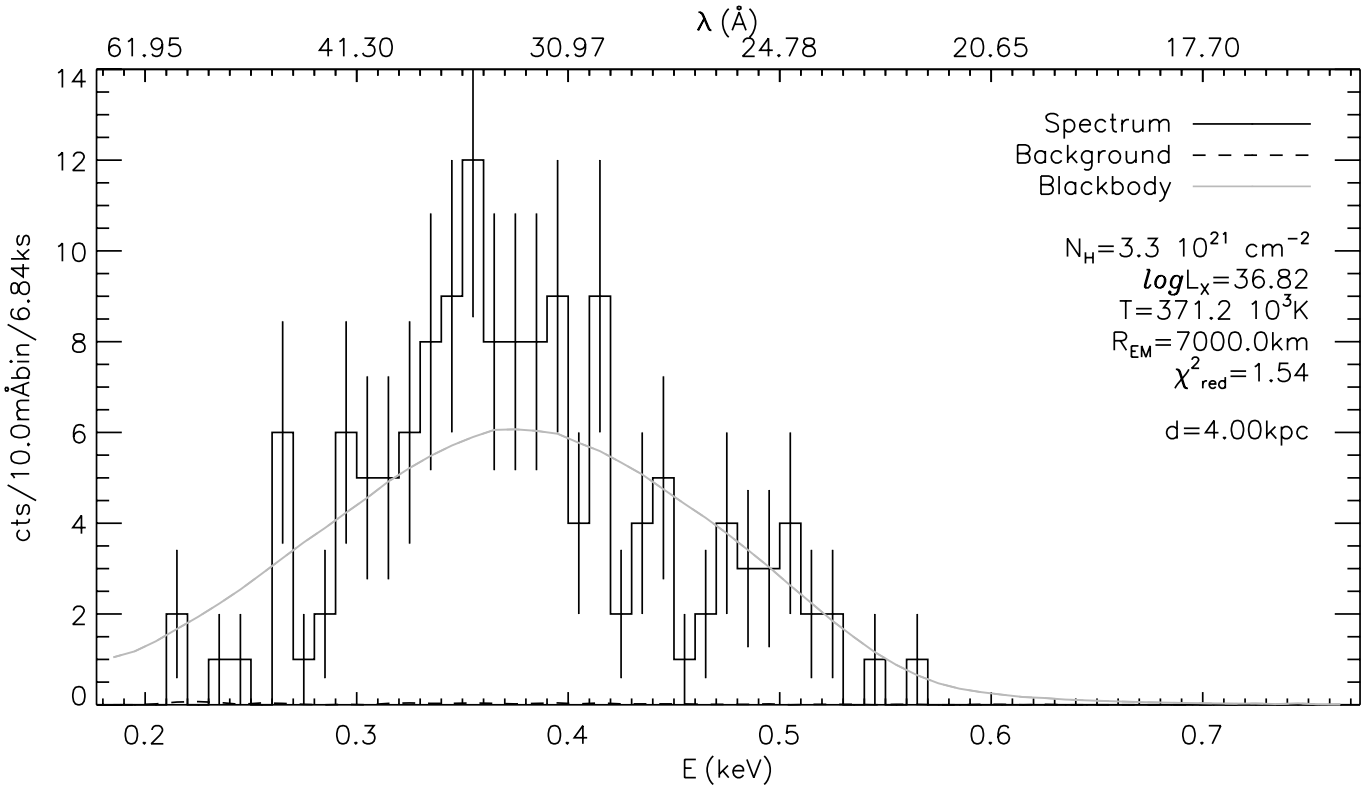

FIG. 6.—Blackbody fit to the XRT spectrum of V723 Cas. The background lies on top of the horizontal axis.

From MOS1, we extracted 0.11 ± 0.002 counts s^{-1} for V4743 Sgr. The source was also detected in the RGS with a count rate of 0.01 ± 0.0005 counts s^{-1}. Grating spectra allow the calculation of a flux without the need of a model, and we measured a flux of 3×10^{-13} erg cm^{-2} s^{-1} from the RGS1 and RGS2.[9]

4. DISCUSSION

The sample of X-ray observations of novae presented in this paper demonstrates that *Swift* significantly increased the number of Galactic novae observed in X-rays. We provide a large sample taken with the same instrument, which reduces problems from cross calibration. Also, *Swift* is capable of carrying out monitoring observations with relatively little effort, the exception being classical novae with large column densities. In § 2.2 we demonstrated that when the column density exceeds $N_H > 10^{22}$ cm^{-2}, one cannot obtain enough counts in a typical ToO exposure (3–5 ks) to observe an SSS phase. In this survey, the estimated column densities of four novae, V382 Nor, V1047 Cen, V1663 Aql, and V476 Sct, exceeded this value and only very hard spectra or nondetections were recorded. For Galactic novae with low column densities, *Swift* is an excellent instrument for following all the stages of evolution in X-rays (e.g., the recurrent nova RS Oph; J. P. Osborne et al. 2007, in preparation).

Shortly after the outburst, X-ray emission from the WD is not expected to be observed. X-ray detections during this phase thus originate from other processes, e.g., shocks within the expanding shell or a shock set off by a collision between the expanding shell and the atmosphere of the companion (as in RS Oph; e.g., Bode et al. 2006). Few observations during this phase have been carried out (e.g., Mukai & Ishida 2001), and they only provide information on dynamics within the ejecta. With the flexibility of *Swift*, a better assessment of pre-SSS X-ray emission can be achieved.

The SSS phase is the brightest phase of X-ray emission (at constant bolometric luminosity), making it the best time to observe a nova. We found two clear detections of novae in this phase. With these two new SSS spectra, the number of Galactic novae clearly observed in this state is seven (Orio et al. 2001a; Drake et al. 2003; Ness et al. 2003, and references therein). For V574 Pup, we were even able to identify the transition from an early emission-line spectrum to a bright SSS spectrum within two months. V574 Pup entered its SSS phase within 250 days after outburst. This is consistent with the evolution of V1974 Cyg, V1494 Aql, and V4743 Sgr (see Fig. 7). The detection of a SSS in V723 Cas suggests that nuclear burning is still going on more than 11 years after outburst. It is not known how much longer it will remain a SSS. More detailed discussions on V723 Cas will be presented by J.-U. Ness et al. (2007, in preparation).

We detected V4743 Sgr 2 years after *XMM-Newton* had already measured a very low level of X-ray emission (see § 3.4). This shows that the post-turnoff evolution can last a few years. V1494 Aql was not detected, but 5 years prior to our observation, it had been found to have marginal emission and no SSS spectrum.

In order to compare the evolution of the novae detected in our sample, we plot their distance-scaled X-ray brightnesses as a function of individual time after outburst in Figure 7. In the bottom panel, we show the X-ray light curves (in the same time units) of five more Galactic novae, but observed by different missions. The brightness is given as unabsorbed luminosity as extracted from direct measurements of fluxes (Greiner et al. 2003; Orio et al. 2001b; Balman et al. 1998; Ness et al. 2003; Petz et al. 2005). As a general rule, any X-ray detection of novae earlier than 100 days after outburst arises from the hard, shock-generated phase that can either

[9] 0.35–1.8 keV; corrected for the chip gaps.

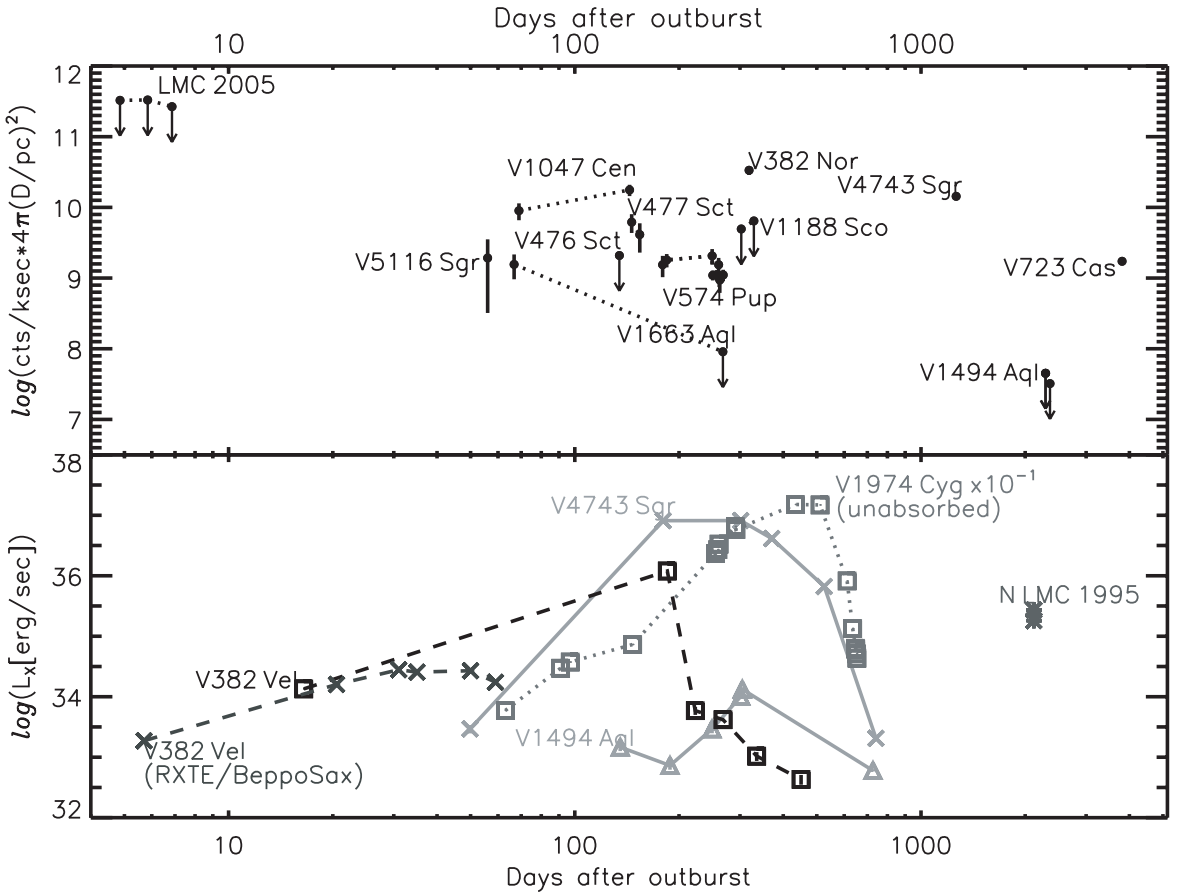

FIG. 7.—*Top*: XRT count rates of all sources in our sample, plotted against the day of observation after their outbursts. The count rates are corrected for distance squared, which is uncertain. Multiple observations of the same targets are connected with dotted lines. *Bottom*: Observations from various other missions. The observed X-ray luminosities (not corrected for absorption, except for V1974 Cyg, which is instead rescaled) of recent well-observed novae with SSS phases. Similar plots have been created by Pietsch et al. (2005, 2006).

be emission lines or possibly bremsstrahlung emission (Orio et al. 2001b; Mukai & Ishida 2001). Likewise, any X-ray detections more than 1000 days after outburst come from the nebular phase, with the three exceptions of GQ Mus, LMC 1995, and now V723 Cas. These general rules also hold for novae in M31 (see Fig. 3 in Pietsch et al. 2005).

Finally, we can use the parameters derived from the model fits to the SSS spectra of V574 Pup and V723 Cas to check the *Swift* counts that we predicted from our attenuated Cloudy model of an "average" classical nova ejection in Figure 2 (§ 2.2). From our blackbody fits, we obtained effective temperatures of $\sim 3 \times 10^5$ K (25 eV) for both novae, while the derived column densities were 2.7 and 1.7×10^{21} cm^{-2} for V574 Pup and V723 Cas, respectively. With these parameters, we find from the grid of Cloudy models (Fig. 2) the predicted counts in a 1 ks observation at a distance of 1 kpc of ~10 for V574 Pup and ~100 for V723 Cas. Scaling these predicted counts by the distances in Table 1 and the exposure times in Table 2 [$(t_{\rm exp}$ ks)/(D kpc^2)] gives 75 counts for V723 Cas and 7 counts for the 2005 July 30 observation of V574 Pup. These values are consistent with the detections, given the uncertainties in the distances and the use of a generalized nova model (e.g., a luminosity of 10^{38} erg s^{-1}, an ejected mass $\sim 10^{-4}\ M_\odot$; Schwarz et al. 2007). For "normal" classical novae, calculations like those done for Figure 2 can be used as a tool to plan X-ray observations by providing first-order estimates of expected X-ray brightness levels during the SSS phase.

We acknowledge the use of public data from the *Swift* data archive. We acknowledge with thanks the variable star observations from the AAVSO International Database contributed by observers worldwide and used in this research. J.-U. N. gratefully acknowledges support provided by NASA through *Chandra* Postdoctoral Fellowship grant PF5-60039 awarded by the *Chandra* X-ray Center, which is operated by the Smithsonian Astrophysical Observatory for NASA under contract NAS8-03060. S. S. received partial support from NSF and NASA grants to ASU. J. P. O. acknowledges support from PPARC.

Facilities: Swift (XRT), XMM, CXO

APPENDIX

EXTRACTION OF SOURCE COUNTS

In this section we give a detailed account of our methods for determining the count rates and detection probabilities. We determined the positions of the sources on the chip from the individual sky coordinates and used circular extraction regions (radius of 10 pixels = 23.6″, which encircles ~80.5% of the total PSF). For the extraction of the background, we defined annular extraction regions around

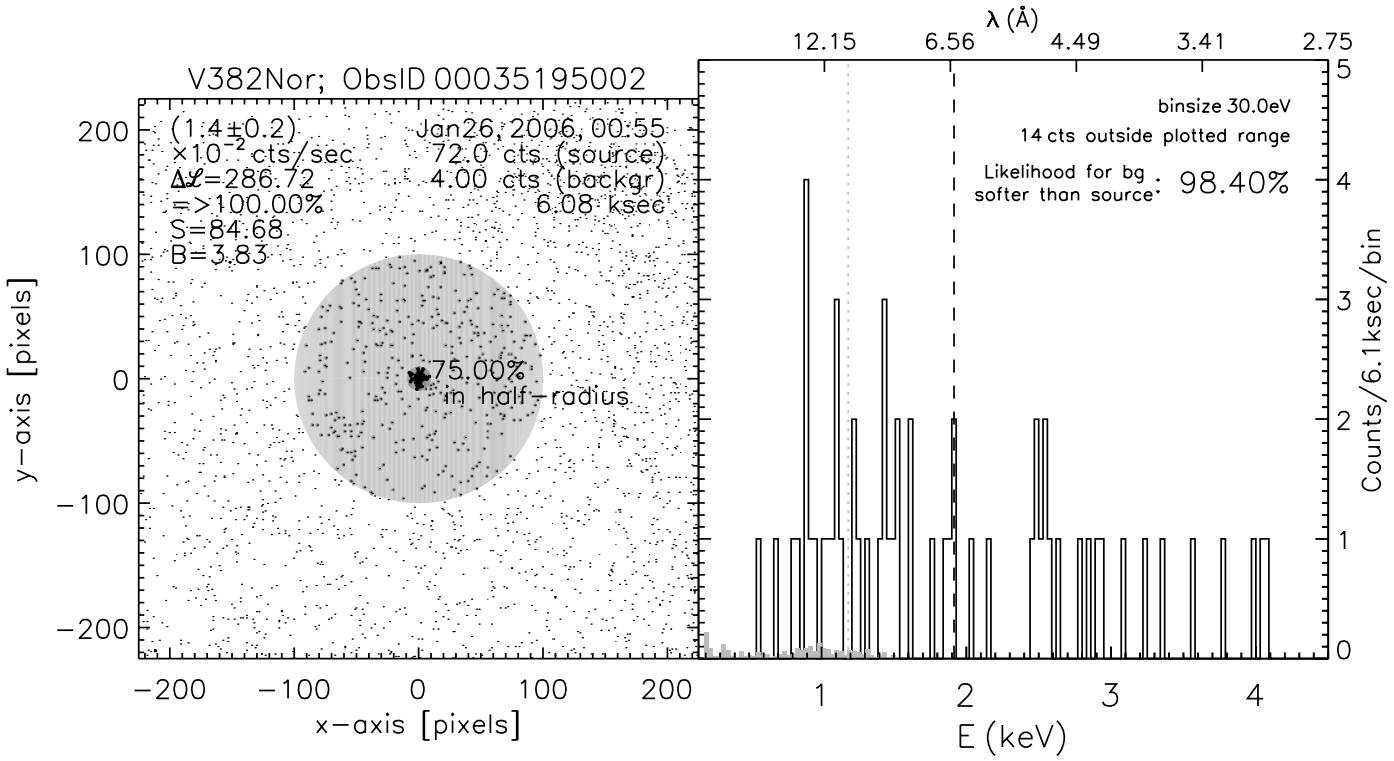

FIG. 8.—Same as Fig. 5, but for V382 Nor. While the count rates are similar, the observed spectra are very different.

the source position with an inner radius of 10 pixels and an outer radius of 100 pixels. We carefully checked to make sure that no sources were present in the background extraction regions. We scaled the number of extracted background counts by the ratio of extraction regions (99.0) to determine the number of expected background counts per detect cell. We assume Poissonian noise and thus apply a maximum likelihood estimation in order to determine the net source count rate. We define two model parameters S and B that represent the number of expected counts of source and background for the source extraction region and calculate the number of expected counts in the source and background extraction regions N_s and N_b:

$$N_s = \alpha S + BN_b = (1-\alpha)S + \beta B, \tag{A1}$$

where $\alpha = 0.80$ is the fraction of the PSF included in the detect cell, and $\beta = 99$ is the ratio of background to source extraction areas. Under the assumption of Poissonian statistics, we can calculate the probability of finding the measured numbers of counts n_s and n_b in the respective extraction regions when S and B are given:

$$P = \frac{N_s^{n_s}}{n_s!} e^{-N_s} \frac{N_b^{n_b}}{n_b!} e^{-N_b}, \tag{A2}$$

and thus the likelihood can be calculated,

$$\mathcal{L} = -2 \ln P = -2n_s \ln(\alpha S + B) - (\alpha S + B) + n_b \ln[(1-\alpha)S + \beta B] - [(1-\alpha)S + \beta B] + \text{const.} \tag{A3}$$

We seek solutions for S and B where $\mathcal{L}$ reaches a minimum, which holds for $N_s = n_s$ and $N_b = n_b$, and thus

$$S = \frac{n_b - \beta n_s}{1 - \alpha - \alpha\beta}, \quad B = \frac{n_s - \alpha(n_s + n_b)}{1 - \alpha - \alpha\beta}, \tag{A4}$$

leading to a minimum value $\mathcal{L}_{\min}$ of

$$\mathcal{L}_{\min} = -2[n_s(\ln n_s - 1) + n_b(\ln n_b - 1)]. \tag{A5}$$

With the definition of $\mathcal{L}$, the range between $\mathcal{L}_{\min}$ and $\mathcal{L}_{\min} + 1$ is equivalent to the 68.3% uncertainty range of the critical parameter S. We thus obtained the formal 1 σ errors by varying S until the value of $\mathcal{L}$ had increased by 1.0 from the minimum while leaving B fixed at the value obtained from equation (A4).

The value of $\mathcal{L}_{\min}$ can also be used to calculate the detection probability (in percent) based on the likelihood ratio test, which is a statistical test of the goodness of fit between two models. A relatively more complex model is compared to a simpler model (null hypothesis) to see if it fits a particular data set significantly better. We define the likelihood for the null hypothesis $\mathcal{L}_0$ as $\mathcal{L}(S = 0)$, and

$$\Delta\mathcal{L} = \mathcal{L}(S) - \mathcal{L}_0 \tag{A6}$$

quantifies the improvement in $\mathcal{L}$ after including $S > 0$. The parameter B is an "uninteresting parameter," as defined by Avni (1976), and we thus convert $\Delta\mathcal{L}$ to the probability for *one* degree of freedom using the IDL[10] function `chisqr_pdf`.

In cases where no counts were found in the detect cell ($n_s = 0$) or when the number of counts in the detect cell was smaller than that expected from the background ($n_s < n_b$), we calculated the 95% upper limits from the number of expected background counts and those actually measured in the detect cell. We again used the likelihood ratio test and solved equation (A6) for $\mathcal{L}(S)$ according to equation (A3), yielding the value of S that returns $\Delta\mathcal{L} = 4$. We also calculated upper limits in cases where the derived 1 σ uncertainties were larger than the measured count rate.

In addition to the formal detection likelihood, we consider whether the photons inside the source extraction region show some concentration toward the center, and whether their energy distribution is different from that of the instrumental background. In order to assess the concentration toward the center, we give the percentage of counts that we found in the central quarter of the detect cell in the last column of Table 2. From the PSF, we expect 60.5% of source photons to be within a circle of radius 5 pixels, and any number much below this fraction is likely not a source. We also studied the spectral energy distribution of the background compared to that of the source as an auxiliary criterion. We computed the median of recorded energies of the source counts and compared with the same value from the background. These values are marked by vertical lines (gray dotted for background and black dashed for source in Figs. 5 and 8). In order to assess the probability that the background spectrum is softer than the source spectrum, we generated 1000 spectra with n_s counts drawn as random subsamples out of the pool of extracted background counts n_b and calculated the median value for each generated spectrum. While a situation in which 50% of all random cases return lower median energies does not imply a nondetection, any strong deviation from 50% is supportive of an independent source spectrum.

[10] Interactive Data Language, ITT Corporation.

REFERENCES

Avni, Y. 1976, ApJ, 210, 642
Balman, S., Krautter, J., & Ögelman, H. 1998, ApJ, 499, 395
Bode, M. F., et al. 2006, ApJ, 652, 629
Burrows, D. N., et al. 2005, Space Sci. Rev., 120, 165
Della Valle, M., & Livio, M. 1995, ApJ, 452, 704
Drake, J. J., et al. 2003, ApJ, 584, 448
Ferland, G. J., Korista, K. T., Verner, D. A., Ferguson, J. W., Kingdon, J. B., & Verner, E. M. 1998, PASP, 110, 761
Gallagher, J. S., & Starrfield, S. 1978, ARA&A, 16, 171
Greiner, J., Orio, M., & Schartel, N. 2003, A&A, 405, 703
Iijima, T., & Esenoglu, H. H. 2003, A&A, 404, 997
Iijima, T., Rosino, L., & Della Valle, M. 1998, A&A, 338, 1006
Kiss, L. L., & Thomson, J. R. 2000, A&A, 355, L9
Krautter, J., Ögelmann, H., Starrfield, S., Wichmann, R., & Pfeffermann, E. 1996, ApJ, 456, 788
Lane, B. F., Retter, A., Eisner, J. A., Thompson, R. R., & Muterspaugh, M. W. 2006, Proc. SPIE, 6268, 161
Lanz, T., Telis, G. A., Audard, M., Paerels, F., Rasmussen, A. P., & Hubeny, I. 2005, ApJ, 619, 517
Lyke, J. E., Kelley, M. S., Gehrz, R. D., & Woodward, C. E. 2002, BAAS, 34, 1161
Moretti, A., et al. 2004, Proc. SPIE, 5165, 232
Mukai, K., & Ishida, M. 2001, ApJ, 551, 1024
Munari, U., Henden, A., Pojmanski, G., Dallaporta, S., Siviero, A., & Navasardyan, H. 2006a, MNRAS, 369, 1755
Munari, U., Siviero, A., Navasardyan, H., & Dallaporta, S. 2006b, A&A, 452, 567
Munari, U., et al. 1996, A&A, 315, 166
Ness, J.-U., Starrfield, S., Jordan, C., Krautter, J., & Schmitt, J. H. M. M. 2005, MNRAS, 364, 1015
Ness, J.-U., et al. 2003, ApJ, 594, L127
———. 2006, IAU Circ., 8676, 2
Orio, M., Covington, J., & Ogelman, H. 2001a, A&A, 373, 542
Orio, M., et al. 2001b, MNRAS, 326, L13
Paerels, F., Rasmussen, A. P., Hartmann, H. W., Heise, J., Brinkman, A. C., de Vries, C. P., & den Herder, J. W. 2001, A&A, 365, L308
Perry, R. B., Venturini, C. C., Rudy, R. J., Mazuk, S., Lynch, D. K., Puetter, R. C., & Walp, B. 2005, IAU Circ., 8638, 1
Petz, A., Hauschildt, P. H., Ness, J.-U., & Starrfield, S. 2005, A&A, 431, 321
Pietsch, W., Fliri, J., Freyberg, M. J., Greiner, J., Haberl, F., Riffeser, A., & Sala, G. 2005, A&A, 442, 879
Pietsch, W., et al. 2007, A&A, 465, 375
Puetter, R. C., Rudy, R. J., Lynch, D. K., Mazuk, S., Venturini, C. C., Perry, R. B., & Walp, B. 2005, IAU Circ., 8640, 2
Rauch, T. 1997, A&A, 320, 237
Schwarz, G. J., Shore, S. N., Starrfield, S., Hauschildt, P. H., Della Valle, M., & Baron, E. 2001, MNRAS, 320, 103
Schwarz, G. J., et al. 2007, ApJ, 657, 453
Shore, S. N., Sonneborn, G., Starrfield, S., Gonzalez-Riestra, R., & Polidan, R. S. 1994, ApJ, 421, 344
Shore, S. N., et al. 2003, AJ, 125, 1507
Siviero, A., Munari, U., & Jones, A. F. 2005, Inf. Bull. Variable Stars, 5638, 1
Starrfield, S. 1992, in Reviews in Modern Astronomy Vol. 5: Variability in Stars and Galaxies, ed. G. Klare (New York: Springer), 73
van den Bergh, S., & Younger, P. F. 1987, A&AS, 70, 125